Materials Science and Engineering A 527 (2010) 3166–3175

Contents lists available at ScienceDirect

Materials Science and Engineering A

journal homepage: www.elsevier.com/locate/msea

# Spherical indentation of metallic foams

Wenyi Yan*, Chung Lun Pun

*Department of Mechanical and Aerospace Engineering, Monash University, Clayton, VIC 3800, Australia*

ARTICLE INFO

*Article history:*
Received 9 November 2009
Received in revised form 21 January 2010
Accepted 21 January 2010

*Keywords:*
Spherical indentation
Metallic foams
Hardness
Finite element simulations

ABSTRACT

Metallic foams are a new class of functional materials. They have found their applications as sandwich cores in lightweight structures and as implant materials in bioengineering. To characterize the mechanical properties of these materials becomes an interesting and relevant research topic. In the mean time, indentation method has been well accepted as a simple and effective way to measure the mechanical properties of solid materials. We believe that it is possible to study the averaged mechanical properties of a metallic foam from a spherical indentation test. In this paper, theoretical investigation to understand the spherical indentation responses of metallic foams is presented. Based on the dimensional analysis, several scaling relationships in the indentation of metallic foams with a spherical indenter are obtained. Numerical results from the finite element simulations are used to examine the dependence of the indentation response on the basic material parameters, such as the porosity, the work hardening exponent and the shape factor, which characterizes the plastic deformation of metallic foams due to hydrostatic loading. Our numerical results show that the maximum indentation force has a linear relationship with the indentation depth for different shape factor values. It is therefore proposed to calibrate the shape factor value from the slope of the maximum indentation force versus the indentation depth from a spherical indentation test, instead of a complicated hydrostatic loading test. We also find that the spherical indentation hardness varies about 11% within the examined indentation depths. The range of the ratio of the hardness to the yield strength of metallic foams is from 2.17 to 2.95, which is different from that of solid materials. Our study provides the basis for applying a simple spherical indentation test to investigate the mechanical properties of metallic foams.



## 1. Introduction

Metallic foams were introduced about 40 years ago [1]. They can be divided into two categories, open cell foams and closed cell foams. The major difference between foam materials and solid materials is their microstructure. A large amount of cells or pores are present in foam materials and their microstructure can be imagined as sponge. Connections of these porous areas range from the near-perfect order of bee's honeycomb to disordered, three-dimensional networks of sponges [2]. Therefore, a metallic foam is characterized microstructurally by its cell topology, relative density, cell size and cell shape. The term, porosity, is a parameter used at the macroscopic scale to indicate the proportion of porous area in foams.

Presence of pores results in metallic foams to be lighter in weight, have lower density and lower stiffness. Due to these characteristics, metallic foams are finding an increasing range of applications in structural engineering. Alporas, the trade name of an aluminium alloy foam, has been applied as sound absorbers along motorways and other busy roads in Japan [3]. In aerospace industry, Boeing has evaluated the use of large titanium foam sandwich parts and aluminium sandwiches with aluminium foam cores for tail-booms of helicopters [3]. Additionally, many potential application concepts are under research and development, e.g. metallic foams as implant materials in bioengineering. In this new area, the most promising application is in orthopedic surgery as load-bearing scaffolds. The Young's modulus of a metallic foam can be tailed easily by choosing a proper porosity so that the stiffness of a foam based implant can match that of the surrounding bone. Such a match can not only avoid bone shrinkage (so called stress shielding problem) after surgical operation but also stimulate bone growth. Another advantage is open cell foam allows possible ingrowth of substantial bone. This would greatly improve the bone–implant interface and may allow for efficient soft tissue attachment [4–6]. As a successful example, titanium foam is used as an interbody fusion device for the human lumbar spine (PlivioPore$^{TM}$) [7].

For a successful application as structural components, knowledge of the plastic yield surface and subsequent plastic flow behaviour of a metallic foam is very important. In contrast to solid metals, metallic foams can yield under hydrostatic loading in addition to deviatoric loading [8]. Therefore, the yield criterion depends on both the von Mises equivalent stress and the mean stress. Two

* Corresponding author. Tel.: +61 3 99020113; fax: +61 3 99051825.
*E-mail address:* wenyi.yan@eng.monash.edu.au (W. Yan).

0921-5093/$ – see front matter © 2010 Elsevier B.V. All rights reserved.
doi:10.1016/j.msea.2010.01.068

phenomenological yield criteria have been used to describe the behaviour of metallic foams [9,10]. Based on the model of Deshpande and Fleck [10], the contribution of the mean stress (pressure stress) on the yield function is realized through a material parameter known as shape factor. It defines the aspect ratio of the elliptical yield surface in the stress plane of von Mises stress versus pressure stress. This shape factor quantitatively distinguishes the plastic behaviour of metallic foams from solid metals. Generally, the shape factor should be determined by performing a hydrostatic compression test, which is relatively complicated.

In the mean time, indentation method has been well accepted as a simple and effective way to study the mechanical properties of solid materials. For example, the hardness and Young's modulus of a material can be obtained from the peak load and the initial slope of the unloading curves using the method of Oliver and Pharr [11,12]. More recently, indentation tests have been used to probe the mechanical properties of some advanced materials and biological materials [13–17]. We believe that indentation test should be able to provide an alternative to study the averaged mechanical properties of metallic foams. To develop an indentation method, it is a prerequisite to understand the effects of material properties on the indentation responses, which is the aim of present study.

Spherical indenter is chosen in our investigation for the purpose of examining the averaged mechanical properties of metallic foams, which obtain the constitutive model developed by Deshpande and Fleck [10]. The finite element method is applied to simulate the spherical indentations. The effects of the basic material properties such as shape factor, porosity and work hardening exponent on the maximum indentation force, initial unloading slope and the hardness analysis are examined from the numerical results.

## 2. Material model for metallic foams

The experimental stress versus strain curves under uniaxial compression for aluminium foams can be found in [1] and for pure titanium foams in [7]. Like ordinal solid metals, a linear elastic region exists at the beginning of the loading. With the increase of external loading, plastic deformation can be observed from the macroscopic stress versus strain curve, as illustrated in Fig. 1(a). At the microscopic scale, this plastic deformation corresponds plastic buckling of cell walls in the foam. Previous research found that the Young's modulus of an open cell metallic foam, $E_f$, and its initial yield strength, $Y_f$, can be estimated, respectively from the foam's porosity, $p_t$, and the Young's modulus, $E_s$, and the initial yield strength, $Y_s$, of the corresponding solid material by [1,2]:

$$E_f = C_1 E_s (1 - p_t)^2, \quad (1)$$

$$Y_f = C_2 Y_s (1 - p_t)^{3/2}, \quad (2)$$

where the porosity, $p_t$, is defined as:

$$p_t = 1 - \frac{\rho_f}{\rho_s}. \quad (3)$$

$\rho_f$ and $\rho_s$ are the density of the foam and the solid, respectively. $C_1$ and $C_2$ are the constants. More complicated formulas for closed cell forms can be found in [2]. Eqs. (1) and (2) are used in our current study with a value of 1.0 for $C_1$ and 0.33 for $C_2$ as suggested by Gibson and Ashby [2].

For the purpose of general parametrical study in this investigation, the hardening function under uniaxial compression is assumed to obey the power law:

$$Y = K\varepsilon^n, \quad (4)$$

where $n$ is the work hardening exponent and $K$ is the work hardening rate determined by $K = Y_f(E_f/Y_f)^n$. Following this power law, the material hardening is defined by the work hardening exponent

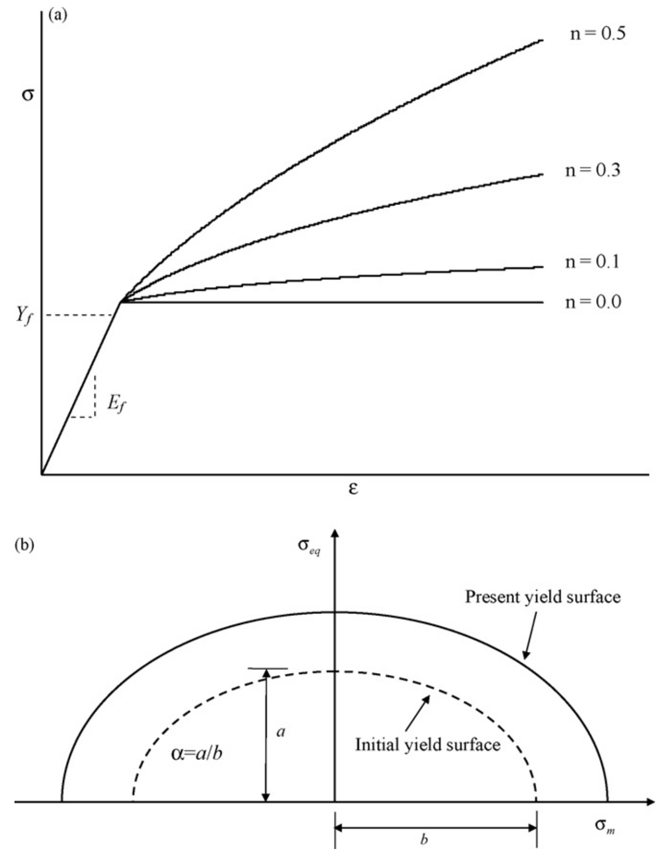


**Fig. 1.** Illustration of the constitutive model for metallic foams: (a) uniaxial stress–strain curves under compression with different hardening exponents; (b) yield surfaces in the stress plane of von Mises stress versus mean stress.

$n$, see Fig. 1(a). If $n$ is equal to zero, there is no hardening and it is called perfect plasticity. For a same solid material, the hardening exponent value can be different for different porosities. The experimental curves in [7] show that the value of $n$ increases from about 0.13 to 0.45 for titanium foams when the foam porosity decreases from 78.7% to 51.5%.

Under three-dimensional loading conditions, a three-dimensional isotropic crushable foam constitutive model was developed and verified by Deshpande and Fleck [10], which was built in the finite element package Abaqus [18] and applied in current study. According to this model, the yield function is:

$$\sqrt{\frac{\sigma_{eq}^2 + \alpha^2\sigma_m^2}{1 + (\alpha/3)^2}} - Y = 0, \quad (5)$$

where $\sigma_{eq}$ is the von Mises equivalent stress and $\sigma_m$ is the mean stress. $Y$ is the material hardening function. Eq. (5) represents an elliptical surface in the stress plane of von Mises stress versus mean stress, as illustrated in Fig. 1(b). The contribution of the mean stress on the macroscopic plastic deformation is quantified by the shape factor $\alpha$ in Eq. (5), which is the aspect ratio of the ellipse. As von Mises stress is a non-negative parameter, only half of the ellipse is illustrated in Fig. 1(b). The influence of the mean stress on the plastic yield of metallic forms increases with the increase in the value of the shape factor. If the shape factor is equal to zero, the von Mises yield criterion is recovered. To avoid negative plastic Poisson's ratio, the reasonable range of $\alpha$ should be between 0 and 2.06. Practically, the shape factor can be calibrated from a hydrostatic compression test. If the ratio of the initial yield stress in uniaxial compression to the initial yield stress in hydrostatic compression is $h$, the value of $\alpha$ is $3h/\sqrt{9 - h^2}$ [18]. Deshpande and Fleck [10] utilized a complex high pressure triaxial testing system to probe the yield surfaces of two aluminium alloy foams and validated this model. This material model has been successfully applied in different problems related to aluminium foams, e.g. [19–22]. Recent study indicates that this model can also be applied to titanium foams [23].

The indentation process is simulated numerically by using the finite element package Abaqus. As mentioned before, a spherical indenter is considered in this study for the purpose of examining the averaged macroscopic properties of metallic foams. Practically, the size of the indenter tip should be reasonably large compared to the size of the cells/pores in the specimen and the indentation depth should also be reasonably large so that the indentation response does reflect the averaged material behaviours, which are described by the aforementioned constitutive model. In reality, the size of the cells varies significantly from foams to foams. For aluminium foams, the cell size is in the range of 2–10 mm [1]. The pore size of the titanium foams studied by Imwinkelried [7] is in the range of 0.1–0.5 mm. In our simulations, the radius of the indenter tip is fixed as 30 mm. In addition, the Young's modulus of an indenter is normally much larger than that of metallic foams, we assume that the indenter is rigid in our theoretical analysis. As the indentation depth and the size of the indentation area are much smaller than the size of the foam specimen, the specimen is treated as a semi-infinite body. Previous studies found that friction has no significant influence on the indentation if the included angle is equal to or higher than 60°, which includes spherical indenter [24,25]. Therefore, a frictionless assumption is made between the indenter and the specimen in our simulations.

Due to the symmetry of this problem, a 2D axisymmetric model is constructed. Fig. 2 illustrates the finite element model. The size of the entire model is much larger than the radius of the indentation tip. The bottom of the model is therefore constrained in both the radial and axial directions. As demonstrated in Fig. 2(b), a very fine mesh with the shortest element side of 0.025 mm is employed in the contact zone beneath the indenter tip to ensure the accuracy of the numerical results. The model contains a total of 47,049 four-noded axisymmetric elements. Testing results for elastic contact are verified by comparison with the Hertz contact theory.

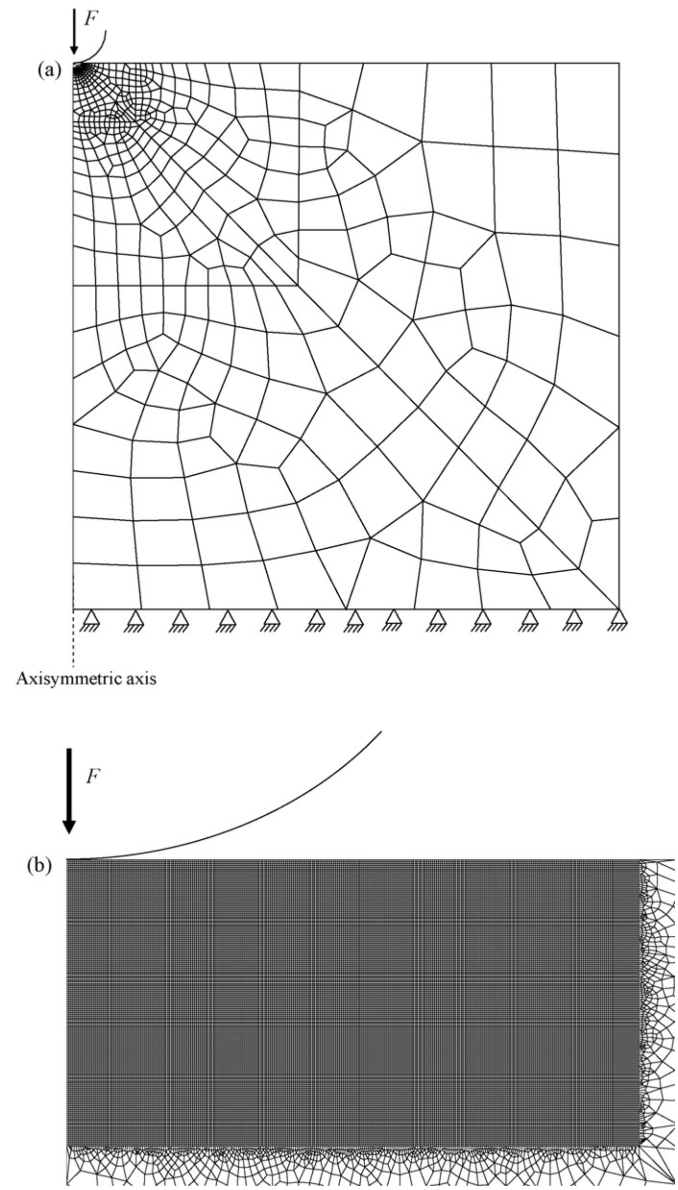


**Fig. 2.** Axisymmetric finite element model to simulate indentation test with a rigid spherical indenter: (a) entire finite element mesh and boundary conditions; (b) fine mesh near the indenter tip.

## 3. Dimensional analysis and numerical results

### 3.1. Maximum indentation force

The indentation force during loading depends on the mechanical properties of the material quantified by the parameters, $E_f$, $Y_f$, $\nu$, $n$, $\alpha$, as well as the indentation depth, $h$, and the indenter radius, $R$, i.e.:

$$F = Z_1(E_f, Y_f, \nu, n, \alpha, h, R). \tag{6a}$$

In order to investigate the influence of porosity, $p_t$, on the indentation response, referring to Eqs. (1) and (2), this functional relationship to determine the indentation loading force can be rearranged as:

$$F = Z_2(E_s, Y_s, p_t, \nu, n, \alpha, h, R). \tag{6b}$$

The parameters, $p_t$ (porosity), $\alpha$ (shape factor), $n$ (work hardening exponent) and $\nu$ (elastic Poisson's ratio), are dimensionless. According to Buckingham $\Pi$ theorem for dimensional analysis, Young's modulus, $E_s$, and the indentation radius, $R$, can be chosen as the primary quantities in this physical problem with two fundamental dimensions, length and force. Therefore, a dimensionless relationship for the indentation loading force can be expressed as:

$$\frac{F}{R^2E_s} = \prod\nolimits_1\left(\frac{Y_s}{E_s}, p_t, \nu, n, \alpha, \frac{h}{R}\right). \tag{7a}$$

The dimensionless function of the maximum indentation force, which is corresponding to the maximum indentation depth, $h_m$, can be presented by:

$$\frac{F_m}{R^2E_s} = \prod\nolimits_1\left(\frac{Y_s}{E_s}, p_t, \nu, n, \alpha, \frac{h_m}{R}\right). \tag{7b}$$

We are interesting in the influence of the shape factor and porosity as well as the work hardening exponent on the indentation response. The elastic Poisson's ratio, $\nu$, is kept constant as 0.3 in this study. Numerical results of the above dimensionless Eq. (7b) are shown in Fig. 3.

Fig. 3(a) shows the relationship between the normalized maximum indentation force and the work hardening exponent under a given shape factor and a given normalized indentation depth. For metallic materials, the work hardening exponent varies between 0 and 0.5. Fig. 3(a) indicates that the normalized maximum indentation force increases with the value of the work hardening exponent almost linearly in all the cases. A higher value of the work hardening exponent means the material is stiffer during plastic deformation

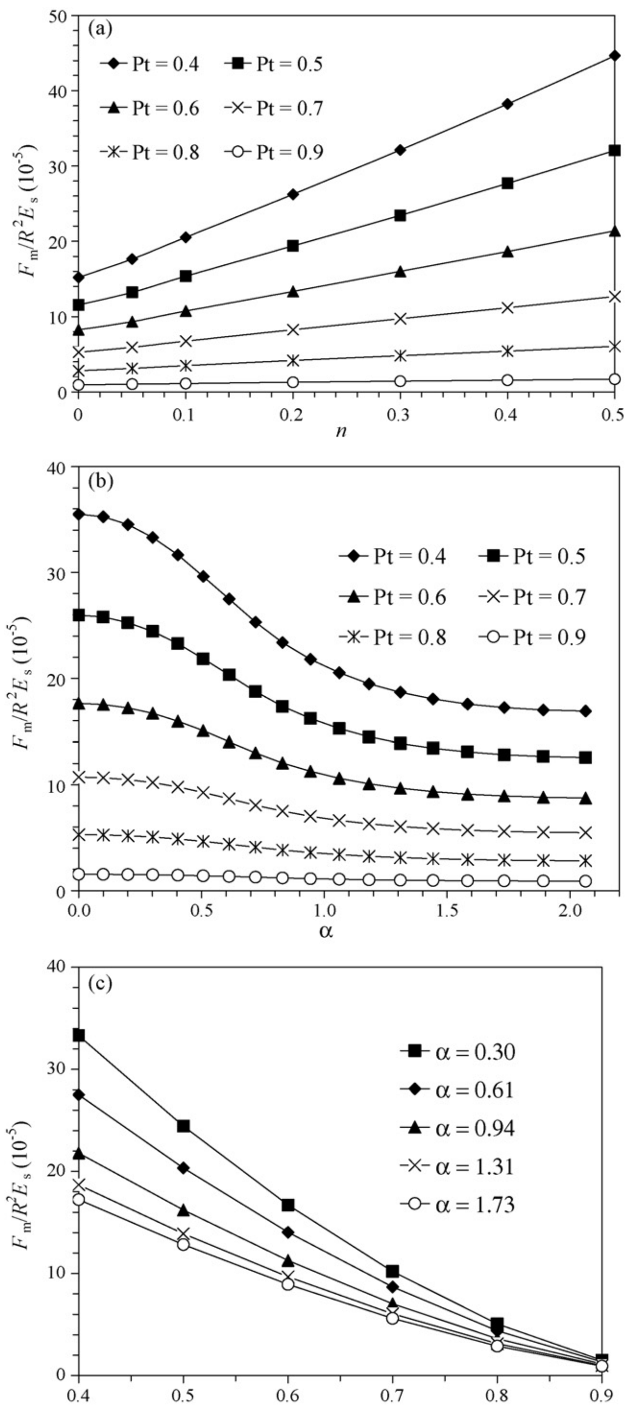


**Fig. 3.** (a) Relationship between the normalized maximum indentation force, $F_m/(R^2E_s)$, and the work hardening exponent, $n$, for different porosities, $p_t$. In all the cases, $Y_s/E_s = 0.00852$, $\alpha = 0.83$, $h_m/R = 0.0133$, $\nu = 0.3$. (b) Relationship between the normalized maximum indentation force, $F_m/(R^2E_s)$, and shape factor, $\alpha$, for different porosities, $p_t$. In all the cases, $Y_s/E_s = 0.00852$, $n = 0.15$, $h_m/R = 0.0133$, $\nu = 0.3$. (c) Relationship between the normalized maximum indentation force, $F_m/(R^2E_a)$, against porosity, $p_t$, for different values of shape factor, $\alpha$. In all the cases, $Y_s/E_s = 0.00852$, $n = 0.15$, $h_m/R = 0.0133$, $\nu = 0.3$.

as illustrated in Fig. 1(a). Therefore, the indenter requires a larger indentation force to reach the same indentation depth. This effect is more significant for materials with a lower porosity ($p_t < 70\%$). Generally, when porosity increases, the influence of the work hardening exponent on the maximum indentation force reduces.

Fig. 3(b) indicates that the normalized maximum indentation force decreases with the increase in the value of the shape factor for different porosities under a given normalized indentation depth. The shape factor represents the contribution of hydrostatic stress on plastic deformation. A higher shape factor value means plastic deformation due to hydrostatic stress can occur more easily in the foam. Therefore, a lower indentation force is required for a given indentation depth. Fig. 3(b) also shows that the influence on the normalized maximum indentation force is mainly significant when the shape factor lies between 0.2 and 1.8 for all the cases with different porosities. When the shape factor is about 0.7, we have the highest decreasing rate of the normalized maximum indentation force. If the shape factor is higher than 1.8, the influence can be neglected. Fig. 3(b) also indicates that influence of the shape factor on the normalized maximum indentation force is more significant in lower porosity foams ($p_t < 70\%$) than that in higher porosity foams ($p_t > 70\%$).

The influence of the porosity on the normalized maximum indentation force is further examined in Fig. 3(c) for different $\alpha$ values. It shows again that the normalized maximum indentation force decreases with the increase in the porosity under these given conditions. This can be explained by the fact that a higher porosity foam has a lower elastic stiffness and a lower yield strength according to Eqs. (1) and (2).

Referring to Eq. (7b), the maximum indentation force is also a function of the maximum indentation depth, $h_m$. Our numerical results indicate that the foam is under pure elastic deformation when the indentation depth is below 0.1–0.15 mm for different porosities. Therefore, the range of the indentation depth of 0.2–0.5 mm is chosen to study its influence on the maximum indentation force. The numerical results for porosity 40%, 60% and 90% are shown in Fig. 4.

Fig. 4(a) shows the relationship between the normalized maximum indentation force and the normalized maximum indentation depth, $h_m/R$, for porosity 40%. It indicates that the normalized maximum indentation force increases with the normalized maximum indentation depth linearly for different shape factors. It is not a surprise that the indenter requires a larger indentation force to reach a larger maximum indentation depth for the same material. It is the linearity sounds interesting. Such linear relationships can also be found from the numerical curves for porosity 60% and 90% with different shape factor values, as shown in Fig. 4(b) and (c). Furthermore, the linear relationship still holds for different work hardening exponent, $n$, in the examples shown in Fig. 4(d). Fig. 4(e) indicates that such a linear relationship is also true for different ratios of yield strength to Young's modulus, $Y_s/E_s$.

According to the numerical curves presented in Fig. 4, one can deduct that the normalized maximum indentation force could be related to the normalized maximum indentation depth by a linear function in general cases, i.e.:

$$\frac{F_m}{R^2E_s} = k \times \frac{h_m}{R}, \tag{8}$$

where the slope $k$ is a function of $Y_s/E_s$, $p_t$, $\nu$, $n$, $\alpha$ according to Eq. (7b). Therefore:

$$k = k\left(\frac{Y_s}{E_s}, p_t, \nu, n, \alpha\right). \tag{9}$$

The linear function (8) is observed from our numerical simulations, where significant plastic deformation occurs. The maximum equivalent plastic strain in the indentation cases presented in Fig. 4 is in the range of 4–20%. In the case of pure elastic contact under small indentation loading condition, an explicit function can be

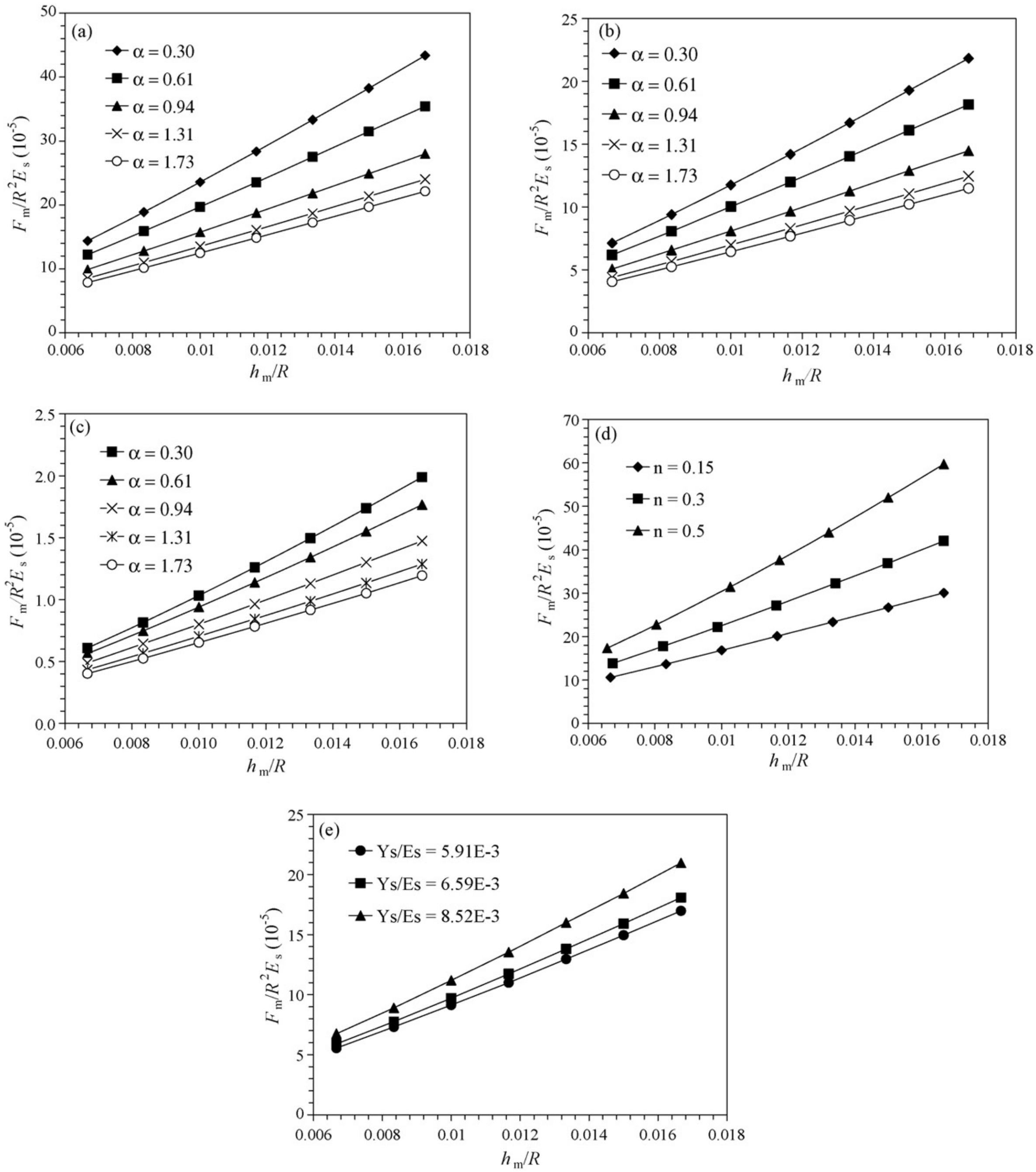


**Fig. 4.** (a) Relationship between the normalized maximum indentation force, $F_m/(R^2E_a)$, and the normalized maximum indentation depth, $h_m/R$, for different values of shape factor, $\alpha$. In all the cases, $Y_s/E_s = 0.00852$, $n = 0.15$, $\nu = 0.3$, $p_t = 0.4$. (b) Relationship between the normalized maximum indentation force, $F_m/(R^2E_a)$, and normalized maximum indentation depth, $h_m/R$, for different values of shape factor, $\alpha$. In all the cases, $Y_s/E_s = 0.00852$, $n = 0.15$, $\nu = 0.3$, $p_t = 0.6$. (c) Relationship between the normalized maximum indentation force, $F_m/(R^2E_a)$ and the normalized maximum indentation depth, $h_m/R$ for different values of the shape factor, $\alpha$. In all the cases, $Y_s/E_s = 0.00852$, $n = 0.15$, $\nu = 0.3$, $p_t = 0.9$. (d) Relationship between the normalized maximum indentation force, $F_m/(R^2E_a)$ and the normalized maximum indentation depth, $h_m/R$ for different work hardening exponent, $n$. In all the cases, $Y_s/E_s = 0.00852$, $\nu = 0.3$, $\alpha = 0.83$, $p_t = 0.4$. (e) Relationship between the normalized maximum indentation force, $F_m/(R^2E_a)$ and the normalized maximum indentation depth, $h_m/R$ for different ratio of yield strength to young's modulus of ordinary solid material, $Y_s/E_s$. In all the cases, $n = 0.3$, $\nu = 0.3$, $\alpha = 0.83$, $p_t = 0.6$.

found from Hertz contact theory and it shows [26,27]:

$$\frac{F_m}{R^2E_s} \propto \left(\frac{h_m}{R}\right)^{1.5}. \tag{10a}$$

If a spherical indentation response is dominated by plastic deformation, the following relationship has been derived for solid elastic–plastic materials under the conditions of neglecting elastic effect and considering small deformation [28,29]:

$$\frac{F_m}{R^2E_s} \propto \left(\frac{h_m}{R}\right)^{\frac{2+n}{2}}. \tag{10b}$$

Even if elasticity and finite deformation are considered, numerical results further indicate that Eq. (10b) still holds under the condition that $h_m/R$ is smaller than about 0.02 for solid elastic–plastic materials [29]. For materials with a weak work hardening, i.e., $n$ has a small value (see Fig. 1(a)), Eq. (10b) can be approximated by the linear Eq. (8). In fact, published spherical indentation loading curves of solid materials from experimental tests demonstrate the linear relationship after an initial nonlinear stage, which is dominated by elastic deformation, e.g. [30,31]. Therefore, besides our numerical results, previous theoretical, numerical and experimental studies on spherical indentation of solid materials do support the linear Eq. (8) under the condition of significant plastic deformation, which means that the indentation depth should be significantly large. Of course, future experimental verification of this linear relationship for metallic foams is required.

Figs. 4(a)–(c) confirm that there is a strong influence of the shape factor, $\alpha$, on the slope, $k$. In fact, these curves show that $k$ reduces with the increase of $\alpha$. We might be able to determine the shape factor, $\alpha$, of the foam from the measured slope, $k$, from spherical indentation tests on the material, if we could find the inverse relationship of Eq. (9), i.e.:

$$\alpha = \alpha\left(\frac{Y_s}{E_s}, p_t, \nu, n, k\right). \tag{11}$$

For a given solid material, the ratio, $Y_s/E_s$ is known and assume that the Poisson's ratio is a constant, say 0.3. If the porosity, $p_t$ and work hardening exponent, $n$, are known, the relationship (11) can be found numerically and used to estimate the shape factor, $\alpha$. As examples, for a given $n = 0.15$, the numerical relationship (11) for different porosities is shown in Fig. 5. Here, all the set of data for different porosities can be fitted by the following rational functions:

$$\alpha = \frac{0.8332k^5 + 1.299k^4 + 10.46k^3 - 1.122k^2 + 0.03327k - 2.632\times10^{-4}}{k^4 - 19.8k^3 + 0.7987k^2 - 0.003035k - 5.411\times10^{-5}} \quad \text{for } p_t = 40\%, \tag{12}$$

$$\alpha = \frac{0.3081k^5 + 1.105k^4 + 8.562k^3 - 0.5021k^2 + 0.007907k - 3.331\times10^{-5}}{k^4 - 21.08k^3 + 0.4823k^2 - 0.001977k - 2.591\times10^{-6}} \quad \text{for } p_t = 60\%, \tag{13}$$

$$\alpha = \frac{0.1366k^5 + 0.7212k^4 + 0.09278k^3 - 2.953k^2 + 0.006196k - 2.731\times10^{-6}}{k^4 + 0.7058k^3 - 2.361k^2 + 0.006006k - 3.09\times10^{-6}} \quad \text{for } p_t = 90\%. \tag{14}$$

It is worthy to mention that these three equations or Fig. 5 are only valid for the corresponding porosity, 40%, 60% and 90% and for a given $n = 0.15$.

For a given porosity 40%, the relationship (11) for different values of work hardening exponent can also be found numerically, as shown in Fig. 6. These curves can be fitted by the following rational functions:

$$\alpha = \frac{0.7237k^5 + 0.2012k^4 + 3.101k^3 - 0.5284k^2 + 0.02237k - 2.539\times10^{-4}}{k^4 - 4.306k^3 + 0.177k^2 + 0.002665k - 8.897\times10^{-5}} \quad \text{for } n = 0.3, \tag{15}$$

$$\alpha = \frac{0.6469k^5 + 0.05951k^4 - 0.486k^3 - 8.296k^2 + 0.5271k - 5.611\times10^{-3}}{k^4 - 1.382k^3 - 12.76k^2 + 1.071k - 0.02013} \quad \text{for } n = 0.5. \tag{16}$$

Eqs. (15) and (16) are only valid, respectively, for $n = 0.3$ and $n = 0.5$ for porosity 40%. Future experimental test is required to validate the linear relation (8) and the accuracy of this proposed method to calibrate the shape factor from a spherical indentation test.

### 3.2. Initial unloading slope

When the spherical indenter reaches the maximum indentation depth in an indentation test, the loading process is finished and it is then followed by an unloading process. During the unloading, the indenter is returning to its original position and elastic deformation in the material is recovering. At the initial unloading stage, plastic deformation will not occur. Our numerical results have confirmed that the plasticity-related parameters, the shape factor, $\alpha$, and the work hardening exponent, $n$, do not affect the initial unloading slope. Therefore, a functional relationship can be obtained:

$$\frac{S}{RE_s} = \prod\nolimits_2\left(\frac{Y_s}{E_s}, p_t, \nu, \frac{h_{\max}}{R}\right), \tag{17}$$

where $S$ is known as the initial unloading slope and is defined as:

$$S = \frac{dF}{dh}\Big|_{h=h_{\max}}. \tag{18}$$

The influence of the porosity on the normalized initial unloading slope is numerically shown in Fig. 7. The normalized initial unloading slope decreases with the increase in the porosity. According to Eq. (1), a higher porosity material has a lower Young's modulus. Therefore, a larger proportion of elastic deformation recovers at this initial unloading stage, which leads to a lower initial unloading slope value. Fig. 7 indicates that the normalized initial unloading slope will also be influenced by indentation depth and it increases with the maximum indentation depth. When the normalized maximum indentation depth increases from 0.01 to 0.017, the normalized initial unloading slope is increased by 31.3% for the porosity 40% and by 33.7% for the porosity for the porosity 90% materials.

The initial unloading slope is also known as the elastic unloading stiffness, which can be applied to measure the Young's modulus of the specimen for ordinary solid materials via [11]:

$$E_f = \frac{1}{\beta}\frac{\sqrt{\pi}}{2}\frac{S}{\sqrt{A}}(1-\nu^2), \tag{19}$$

where $A$ is the contact area and $\beta$ is a constant and a value of 1.05 was suggested [12].

The numerical results of the Young's modulus predicted by Eq. (19) are shown in Fig. 8 and compared with the input data determined by Eq. (1). Fig. 8 clearly shows that the predicted results of the Young's modulus of the metallic foams agree very well with the input data. The largest difference is not more than 2%, which can be neglected practically. Therefore, we can conclude that Eq. (19) can still be applied to predict the Young's modulus of metallic foams from the initial unloading slope of a spherical indentation curve. It is worth mentioning that the contact area $A$ is estimated from finite element output in our numerical predictions not from analyzing the initial unloading slope using the Oliver–Pharr's method. As we know, Oliver–Pharr's method to predict the contact area is only suitable for the cases of "sinking-in". Practically, if "piling-up" of the surface around the indenter occurs, one should use Oliver–Pharr's method with caution. If "piling-up" is large, the image should be used to measure the contact area as suggested by Hay and Pharr [32].

For solid elastic-plastic materials, the degree of "sinking-in" or "piling-up" depends on the plastic yield stress and the level of the strain-hardening [33]. Here, we can numerically examine the influence of foam properties on the spherical indentation phenomenon of "sinking-in" or "piling-up". If the dimensionless contact depth

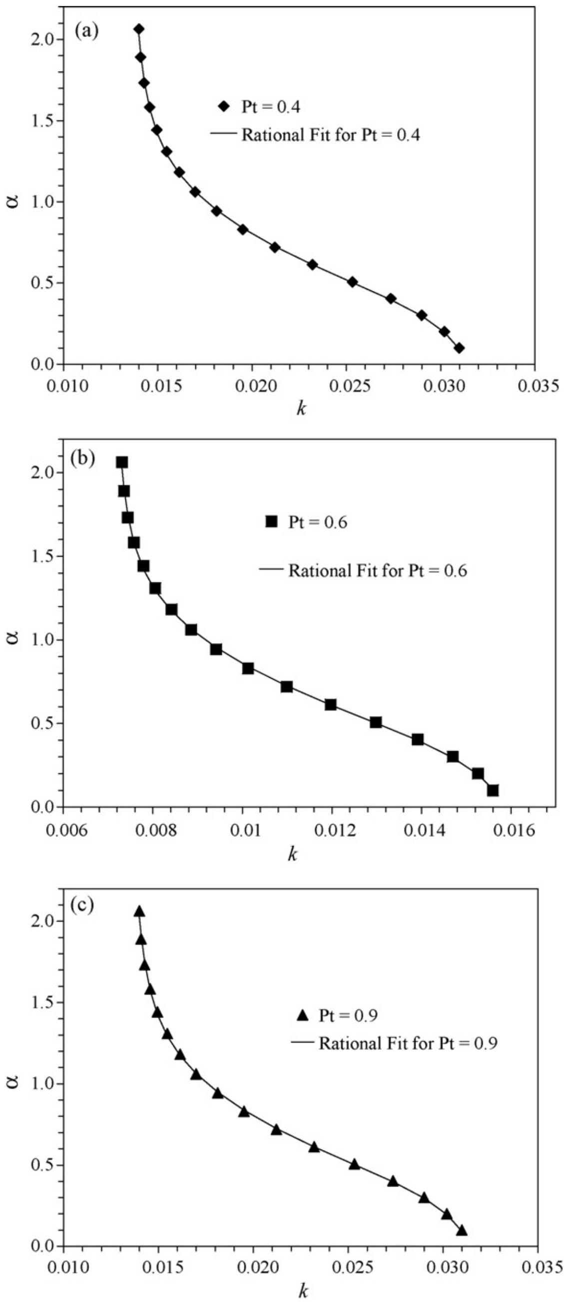


**Fig. 5.** Numerical relationship between the shape factor and the slope of $F_m/(R^2E_a)$ versus $h_m/R$ curve for $Y_s/E_s=0.00852$, $n=0.15$, $\nu=0.3$ and (a) $p_t=0.4$; (b) $p_t=0.6$; (c) $p_t=0.9$.

$h_c/h_m$ is smaller than 1.0, then we have "sinking-in". Otherwise, it is "piling-up" [34,35]. The dependences of $h_c/h_m$ on the shape factor, $\alpha$, the porosity, $p_t$, and the work hardening exponent, $n$, are shown in Figs. 9(a), (b) and (c), respectively. As we can see, in all the studied cases, the dimensionless contact depth, $h_c/h_m$, is smaller than 1.0. We will expect "sinking-in" of the surface around the indenter in a spherical indentation test of a metallic foam. Therefore, we can use Oliver–Pharr's method to predict the contact area and the Young's modulus of the foam.

### 3.3. Spherical indentation hardness

Measurement of material's hardness is one of the major purposes of an indentation test. Hardness indicates material's resistance to plastic deformation and can be defined as:

$$H=\frac{F_m}{A}, \tag{20}$$

where $F_m$ is the maximum indentation force and $A$ is the corresponding projected contact area under the maximum indentation force. According to this definition, the influence of the material's

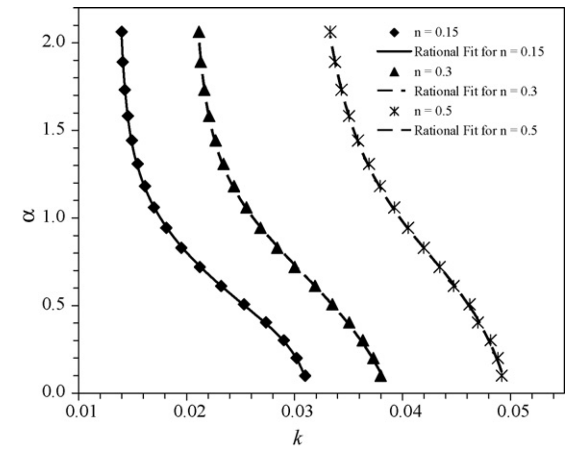


**Fig. 6.** Numerical relationship between the shape factor and the slope of $F_m/(R^2E_a)$ versus $h_m/R$ curve for $n=0.15$, 0.3 and 0.5. In all the cases, $Y_s/E_s=0.00852$, $p_t=0.4$, $\nu=0.3$.

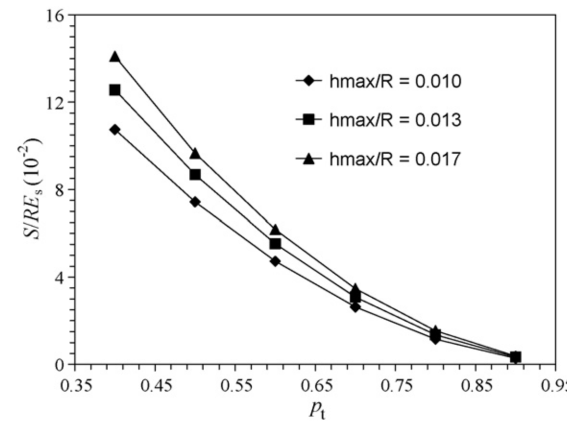


**Fig. 7.** Relationship between the normalized initial unloading slope, $1/(RE_s)(dF/dh)|_{h=h\max}$ and the porosity, $p_t$, for different normalized maximum indentation force, $h_m/R$. In all the cases, $Y_s/E_s=0.00852$, $\nu=0.3$, $\alpha=1.06$ and $R=30$ mm.

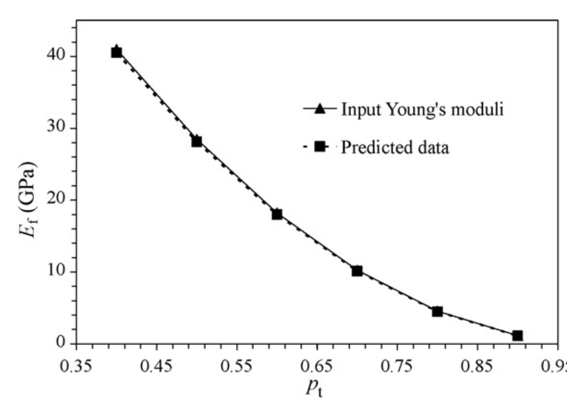


**Fig. 8.** Comparison between input data of the Young's modulus from Eq. (1) for different porosities and the predicted values from Eq. (19). In all the cases, $Y_s/E_s=0.00852$, $\nu=0.3$ and $h_m/R=0.0133$.

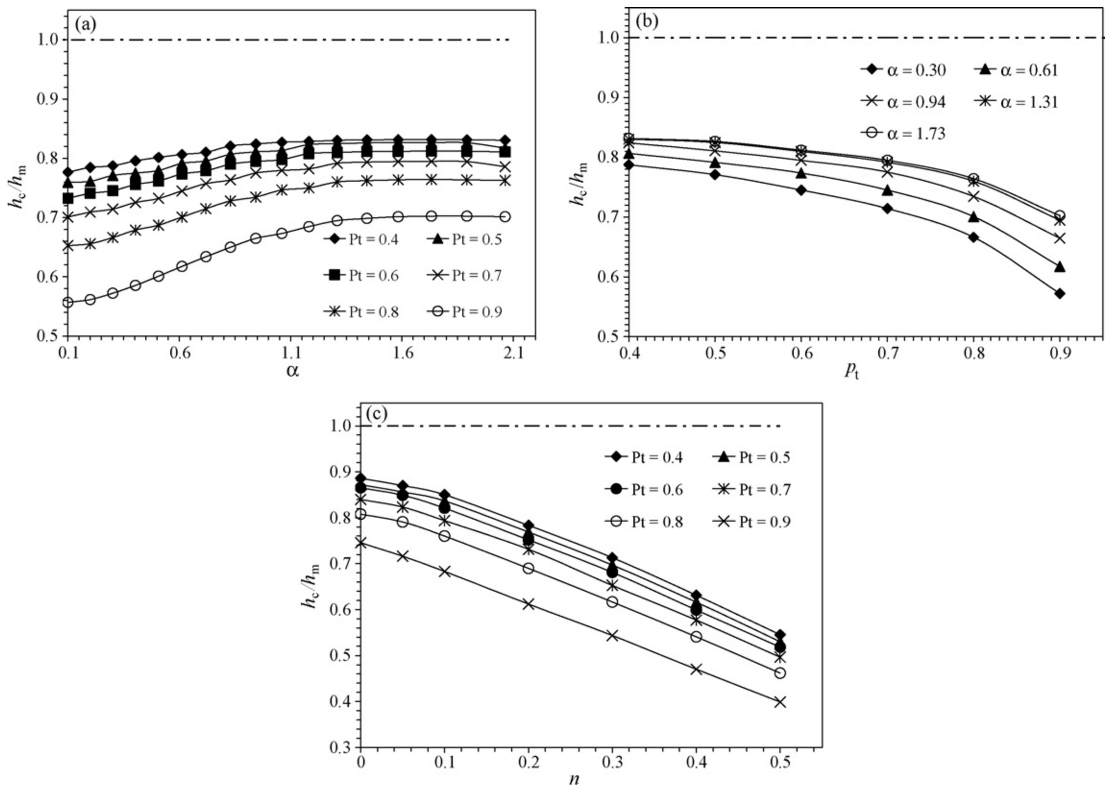


**Fig. 9.** Dependence of the degree of "sinking-in", i.e., $h_c/h_m < 1$, on the foam properties: (a) shape factor, $\alpha$, with $Y_s/E_s = 0.00852$, $n = 0.15$, $\nu = 0.3$, $h_m/R = 0.0133$; (b) porosity, $p_t$, with $Y_s/E_s = 0.00852$, $n = 0.15$, $\nu = 0.3$, $h_m/R = 0.0133$ and (c) work hardening exponent, $n$, with $Y_s/E_s = 0.00852$, $\alpha = 0.83$, $\nu = 0.3$, $h_m/R = 0.0133$.

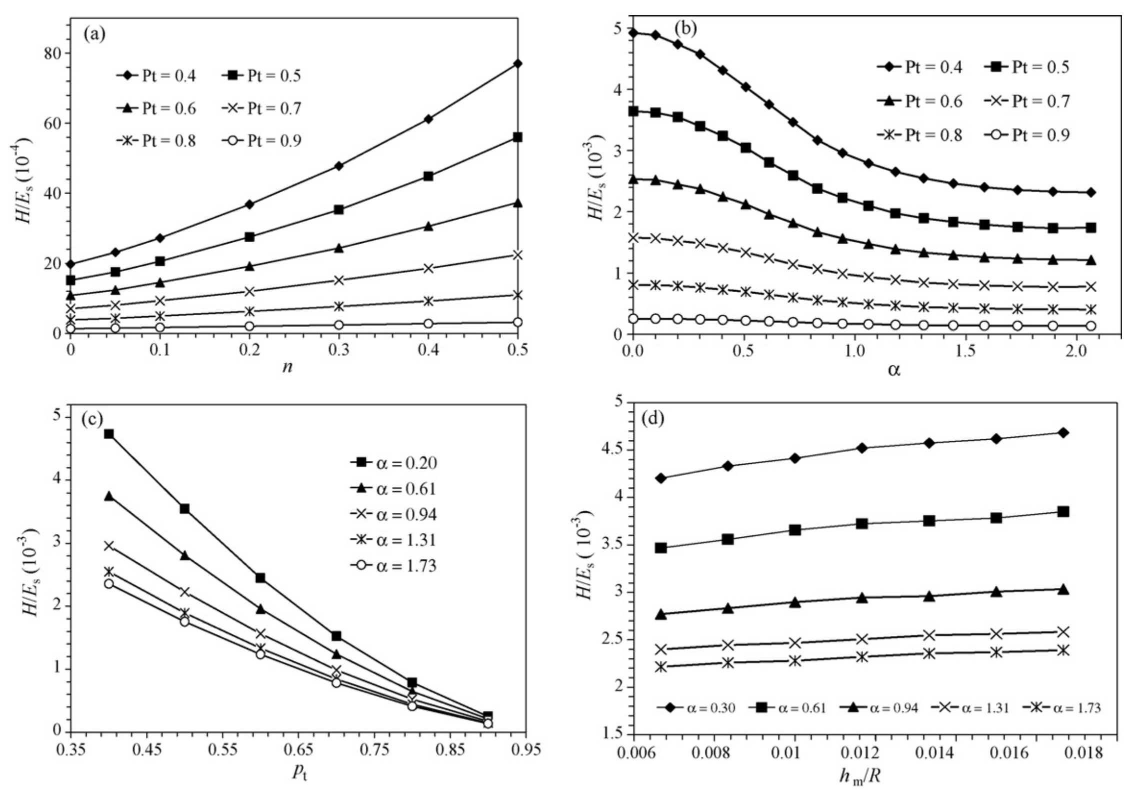


**Fig. 10.** (a) Relationship between the normalized hardness, $H/E_s$, and the work hardening exponent, $n$, for different porosity values. In all the cases, $Y_s/E_s = 0.00852$, $\alpha = 0.83$, $\nu = 0.3$, $h_m/R = 0.0133$. (b) Relationship between the normalized hardness, $H/E_s$, and the shape factor, $\alpha$, for different porosity values. In all the cases, $Y_s/E_s = 0.00852$, $n = 0.15$, $\nu = 0.3$, $h_m/R = 0.0133$. (c) Relationship between the normalized hardness, $H/E_s$, and the porosity values, $p_t$, for different values of shape factor. In all the cases, $Y_s/E_s = 0.00852$, $n = 0.15$, $\nu = 0.3$, $h_m/R = 0.0133$. (d) Relationship between the normalized hardness, $H/E_s$, and the normalized maximum indentation depth, $h_m/R$, for different values of shape factor. In all the cases, $Y_s/E_s = 0.00852$, $n = 0.15$, $\nu = 0.3$, $p_t = 0.4$.

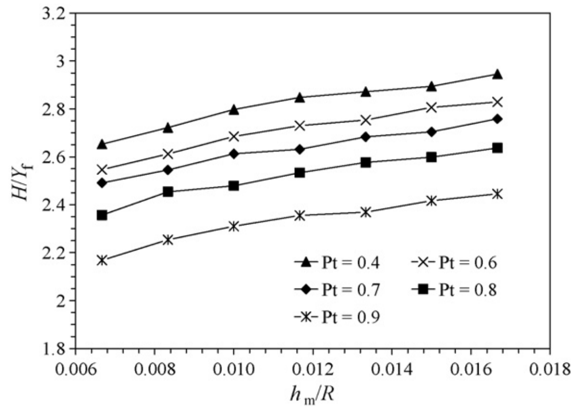


**Fig. 11.** Relationship between the ratio of hardness to yield strength of foam materials, $H/Y$, and the normalized maximum indentation depth, $h_m/R$. In all the cases, $n = 0.15$, $\nu = 0.3$ and $\alpha = 0.61$.

basic parameters on the hardness can be expressed by the following dimensionless function:

$$\frac{H}{E_s} = \prod\nolimits_3 \left( \frac{Y_s}{E_s}, p_t, \nu, n, \alpha, \frac{h_m}{R} \right). \tag{21}$$

The numerical results of above dimensionless function are shown in Fig. 9. Fig. 10(a) indicates that the normalized hardness, $H/E_s$, increases with the work hardening exponent. Furthermore, this influence decreases with the increase of the porosity value. Fig. 10(b) shows the relationship between the normalized hardness and the shape factor. It indicates that the normalized hardness decreases with the increase in the shape factor value. Referring to the material model discussed in previous section, a higher shape factor value means that the plastic deformation due to hydrostatic pressure is more significant, which leads to a lower resistance to plastic deformation and a smaller hardness value. Fig. 10(b) also shows that significant influence occurs when the shape factor lies between 0.2 and 1.5. The maximum decreasing rate occurs when the shape factor value is about 0.8. After this point, the decreasing rate reduced and the normalized hardness settles down to a stable value when the shape factor is larger than 1.8. Furthermore, the graph shows that there is more demonstrative influence on the normalized hardness for lower porosity values ($p_t < 70\%$) than that for higher porosity values ($p_t > 70\%$).

Fig. 10(c) further demonstrates the relationship between the normalized hardness and the porosity. It clearly shows that the normalized hardness decreases with the increases of the porosity. This is due to the fact that a higher porosity material has a lower plastic yield strength according to Eq. (2). Fig. 10(d) shows the relationship between the normalized hardness and the normalized maximum indentation depth. It indicates that the influence of the normalized maximum indentation depth on the normalized hardness is not significant. For all the examined cases, the maximum hardness increase is about 11% when the normalized maximum indentation depth changes from 0.0067 to 0.017. Therefore, for a given metallic foam, the spherical indentation hardness can still be treated roughly as a constant.

Previous study on ordinary elastic–plastic materials found that the hardness ($H$) is about 2.4–2.8 of the yield strength ($Y$) for $Y/E < 0.02$ and it approaches 1.7 for $Y/E > 0.06$ [36]. The numerical ratios of the hardness to the yield strength of metallic foams are shown in Fig. 11. In all these cases, $Y_f/E_f < 0.01$. As we can see, $H/Y_f$ varies from 2.17 to 2.45 for $p_t = 0.9$ and from 2.65 to 2.95 for $p_t = 0.4$. The range of this ratio is different from that of the solid elastic–plastic materials.

## 4. Conclusions

Dimensional analysis and finite element simulations were employed to study the spherical indentation of metallic foams. Several scaling functions were derived to describe the relationships between the indentation responses and the material properties. Our numerical results revealed the influences of the porosity, the shape factor and the work hardening exponent on the indentation responses. The maximum indentation force decreases with the increase of the shape factor and/or the porosity. These influences are more demonstrative for low porosity foams than that for high porosity foams. Furthermore, the maximum indentation force has a linear relationship with the indentation depth for different shape factor values. The slope of such linear curves depends on the shape factor, the porosity, the work hardening exponent and the Poisson's ratio. It is proposed to calibrate the shape factor from the measured slope value from a spherical indentation test if all the other parameters are known or measured from other tests.

Initial unloading slope was also examined in our study. It decreases with the increase of the porosity. Moreover, our numerical results confirmed that the initial unloading slope method for ordinary solid materials can also be applied to calibrate the Young's modulus of metallic foams. The influences of both the shape factor and the porosity on hardness are similar to the influences on the maximum indentation force. We also found that the spherical indentation hardness varies about 11% within the examined indentation depths for the foams with different porosities, shape factors and work hardening exponents. Therefore, the spherical indentation hardness of a metallic foam can still be treated as a constant. The ratio of the hardness to the yield strength of metallic foams varies from 2.17 to 2.95, which is different from that of solid elastic–plastic materials.

## Acknowledgments

The authors would like to acknowledge the financial support from the Australian Research Council (Project No: DP0770021). This research was undertaken on the NCI National Facility in Canberra, Australia, which is supported by the Australian Commonwealth Government.

## References


[1] L.J. Gibson, Annu. Rev. Mater. Sci. 30 (2000) 191–227.
[2] L.J. Gibson, M.F. Ashby, Cellular Solids: Structure and Properties, 2nd ed., Cambridge University Press, Cambridge, 1997.
[3] J. Banhart, Prog. Mater. Sci. 46 (2001) 559–632.
[4] C. Wen, Y. Yamada, K. Shimojima, Y. Chino, H. Hosokawa, M. Mabuchi, J. Mater. Res. 17 (2002) 2633–2639.
[5] S. Thelen, F. Barthelat, L.C. Brinson, J. Biomed. Mater. Res. A 69 (2004) 601–610.
[6] E.D. Spoerke, N.G. Murray, G. Naomi, H. Li, L.C. Brinson, D.C. Dunand, S.I. Stupp, Acta Biomater. 1 (2005) 523–533.
[7] T. Imwinkelried, J. Biomed. Mater. Res. A 81 (2007) 964–970.
[8] M.F. Ashby, A.G. Evans, N.A. Fleck, L.J. Gibson, J.W. Hutchinson, H.N.G. Wadley, Metal Foams: A Design Guide, Butterworth-Heinemann, Oxford, 2000.
[9] R.E. Miller, Int. J. Mech. Sci. 42 (2000) 729–754.
[10] V.S. Deshpande, N.A. Fleck, J. Mech. Phys. Solids 48 (2000) 1253–1283.
[11] W.C. Oliver, G.M. Pharr, J. Mater. Res. 7 (1992) 1564–1583.
[12] W.C. Oliver, G.M. Pharr, J. Mater. Res. 19 (2004) 3–20.
[13] K. Tunvisut, N.P. O'Dowd, E.P. Busso, Int. J. Solids Struct. 38 (2001) 335–351.
[14] Y.T. Cheng, C.M. Cheng, Mater. Sci. Eng. A 409 (2005) 93–99.
[15] D.M. Ebenstein, L.A. Pruitt, Nano Today 1 (2006) 26–33.
[16] W. Yan, Q. Sun, X.-Q. Feng, L.M. Qian, Appl. Phys. Lett. 88 (2006) 241912.
[17] W. Yan, Q. Sun, H.-Y. Liu, Mater. Sci. Eng. A 425 (2006) 278–285.
[18] Abaqus version 6.8, Dassault Systèmes Simulia Corp., Providence, RI, USA, 2008.
[19] K. Mohan, Y.T. Hon, S. Idapalapati, H.P. Seow, Mater. Sci. Eng. A 409 (2005) 292–301.
[20] G. Lu, J. Shen, W. Hou, D. Ruan, L.S. Ong, Int. J. Mech. Sci. 50 (2008) 932–943.
[21] T. Liu, Z.C. Deng, T.J. Lu, Int. J. Solids Struct. 45 (2008) 5127–5151.
[22] A.G. Hanssen, Y. Girard, L. Olovsson, T. Berstad, M. Langseth, Int. J. Impact. Eng. 32 (2006) 1127–1144.

[23] S. Kashef, S.A. Asgari, P.D. Hodgson, W. Yan, Adv. Mater. Res. 32 (2008) 237–240.
[24] J.L. Bucaille, S. Stauss, E. Felder, J. Michler, Acta Mater. 51 (2003) 1663–1678.
[25] W. Yan, Q. Sun, H.-Y. Liu, Int. J. Mod. Phys. B 22 (2008) 5957–5964.
[26] K.L. Johnson, Contact Mechanics, Cambridge University Press, London, 1985.
[27] W. Yan, Q. Sun, P.D. Hodgson, Mater. Lett. 62 (2008) 2260–2262.
[28] R. Hill, B. Storakers, A.B. Zdunek, Proc. Roy. Soc. A 436 (1989) 301–330.
[29] S.D. Mesarovic, N.A. Fleck, Proc. Roy. Soc. A 455 (1999) 2707–2728.
[30] E.G. Herbert, W.C. Oliver, G.M. Pharr, Philos. Mag. 86 (2006) 5521–5539.
[31] J.-M. Collin, G. Mauvoisin, O. Bartier, R.E. Abdi, P. Pilvin, Mater. Sci. Eng. A 501 (2009) 140–145.
[32] J.L. Hay, G.M. Pharr, in: H. Kuhn, D. Medlin (Eds.), ASM Handbook, vol. 8, ASM International, Materials Park, OH, 2000, pp. 232–243.
[33] A.E. Giannakopoulos, S. Suresh, Scripta Mater. 40 (1999) 1191–1198.
[34] B. Taljat, G.M. Pharr, Int. J. Solids Struct. 41 (2004) 3891–3904.
[35] G. Kang, W. Yan, Philos. Mag. 90 (2010) 599–616.
[36] Y.T. Cheng, C.M. Cheng, Mater. Sci. Eng. R 44 (2004) 91–149.